Evolution of Electronic Structure in Atomically Thin Sheets of WS_2 and WSe_2

Weijie Zhao,[†,§,#] Zohreh Ghorannevis,[†,§,#] Leiqiang Chu,[†,§] Minglin Toh,[⊥] Christian Kloc,[⊥] Ping-Heng Tan,[¶] and Goki Eda[†,‡,§,*]

[†]Department of Physics, National University of Singapore, 2 Science Drive 3, Singapore 117542, [‡]Department of Chemistry, National University of Singapore, 3 Science Drive 3, Singapore 117543, [§]Graphene Research Centre, National University of Singapore, 6 Science Drive 2, Singapore 117546, [⊥]School of Materials Science and Engineering, Nanyang Technological University, N4.1 Nanyang Avenue, Singapore 639798, and [¶]State Key Laboratory of Superlattices and Microstructures, Institute of Semiconductors, Chinese Academy of Sciences, Beijing 100083, China
[#]These authors contributed equally to this work.

ABSTRACT Geometrical confinement effect in exfoliated sheets of layered materials leads to significant evolution of energy dispersion in mono- to few-layer thickness regime. Molybdenum disulfide (MoS_2) was recently found to exhibit indirect-to-direct gap transition when the thickness is reduced to a single monolayer. Emerging photoluminescence (PL) from monolayer MoS_2 opens up opportunities for a range of novel optoelectronic applications of the material. Here we report differential reflectance and PL spectra of mono- to few-layer WS_2 and WSe_2 that indicate that the band structure of these materials undergoes similar indirect-to-direct gap transition when thinned to a single monolayer. The transition is evidenced by distinctly enhanced PL peak centered at 630 and 750 nm in monolayer WS_2 and WSe_2, respectively. Few-layer flakes are found to exhibit comparatively strong indirect gap emission along with direct gap hot electron emission, suggesting high quality of synthetic crystals prepared by a chemical vapor transport method. Fine absorption and emission features and their thickness dependence suggest a strong effect of Se p-orbitals on the d electron band structure as well as interlayer coupling in WSe_2.

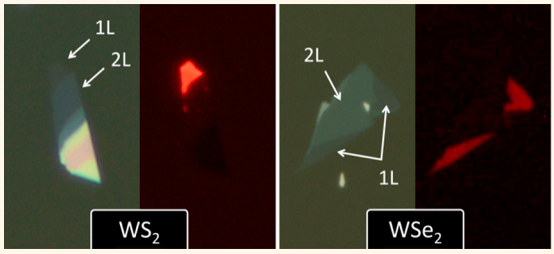

KEYWORDS: WS_2 · WSe_2 · 2D crystals · photoluminescence

Atomically thin sheets of molybdenum disulfide (MoS_2) consisting of a single to a few monolayers were recently found to exhibit a set of unusual properties associated with their two-dimensional (2D) structure and high crystal quality, triggering significant research interest.[1−18] Similar to graphite, MoS_2 crystallizes in a van der Waals layered structure where each layer consists of a slab of S−Mo−S sandwich. Individual monolayers can be mechanically peeled off from a bulk crystal and isolated as a graphene-like 2D crystal.[19] While MoS_2 is traditionally known as a solid-state lubricant and catalyst, its mono- and few-layer crystals hold promise in novel electronic and optoelectronic applications and provides access to fundamental physical phenomena.

Electronically, bulk MoS_2 is an indirect gap semiconductor with the bandgap in the near-infrared frequency range (~1.2 eV).[20] In contrast, monolayer MoS_2 is a direct gap semiconductor with the band gap in the visible frequency range (~1.9 eV).[4,5] Confinement of carriers in the out-of-plane direction induces gradual increase in the band gap with decreasing thickness.[21] The indirect to direct crossover occurs at the monolayer limit resulting in strong contrast in photoluminescence (PL) efficiency between single and multilayer sheets.[4,5] Remarkable electrical properties of mono- and few-layer MoS_2 are increasingly revealed in its field effect transistor characteristics such as exceptionally large on/off ratio, small subthreshold swing, ultralow off-state energy dissipation, high field effect mobility, and large current carrying capacity.[1−3] Explicit inversion symmetry breaking in monolayers allows valley selective pumping of charges using circularly polarized light.[6−8] High electronic quality of the material coupled with thickness-dependent optical properties, mechanical flexibility,[9] and access to valley degree of freedom highlights some of the distinct characteristics of MoS_2 2D crystals.[10−18]

Tungsten-based dichalcogenides such as WS_2 and WSe_2 belong to the same family of

* Address correspondence to g.eda@nus.edu.sg.

Received for review November 13, 2012 and accepted December 19, 2012.

Published online December 19, 2012
10.1021/nn305275h

layered transition metal dichalcogenides (LTMD) as MoS_2.[22] Mechanically exfoliated atomically thin sheets of WS_2 and WSe_2 were recently shown to exhibit high in-plane carrier mobility and electrostatic modulation of conductance similar to MoS_2.[23,24] Both compounds exhibit trigonal prismatic structure and are indirect gap semiconductors in the bulk form with a bandgap of 1∼1.3 eV. The M-M bond length (where M represents a transition metal atom) is nearly identical for MoS_2 (3.16 Å) and WS_2 (3.15 Å) while it is slightly larger for WSe_2 (3.28 Å).[22] Interlayer distance is correspondingly larger for WSe_2 due to the large Se atoms. General features of the WS_2 and WSe_2 band structures are similar to those of MoS_2 where a direct and indirect gap coexist irrespective of thickness.[25−27] A direct gap exists at the K points of the Brilloun zone between the spin−orbit split valence band and the doubly degenerate conduction band. On the other hand, an indirect gap forms between a local conduction band minimum at a midpoint between Γ and K and the valence band maximum at the Γ point. The primary difference between MoX_2 (where X represents a chalcogen atom) and WX_2 is the size of the spin−orbit splitting due to different size of the transition metal atoms.

While MoS_2 2D crystals have been intensively studied in recent years, reports on mono- and few-layer WS_2 and WSe_2 are limited. Here we report differential reflectance and PL spectra of mechanically exfoliated sheets of synthetic 2H-WS_2 and 2H-WSe_2 with thicknesses ranging between 1 and 5 layers. The excitonic absorption and emission bands were found to gradually blueshift with decreasing number of layers due to geometrical confinement of excitons. Strong enhancement in PL efficiency is observed in the monolayers indicating that they are direct gap semiconductors in agreement with the recent experimental findings[28,29] and calculations.[25,26] We show that interlayer coupling effects can be investigated by studying fine absorption and emission features and their dependence on flake thickness. We further demonstrate that the PL emission efficiency of monolayers is higher for synthetic WS_2 and WSe_2 crystals compared to natural MoS_2 crystals.

RESULTS/DISCUSSION

Mechanically exfoliated flakes of WS_2 and WSe_2 were deposited on quartz or SiO_2/Si substrates and their thickness was verified by atomic force microscopy (AFM) and optical contrast (see Supporting Information for AFM images).[30] These samples were chemically stable over 3 months in ambient conditions and showed no obvious sign of degradation according to our Raman analysis.[31] For atomically thin layers supported by a transparent substrate, differential reflectance provides an effective measure of absorbance. The fractional change in reflectance δR for a thin layer sample relative to the reflectance of a dielectric

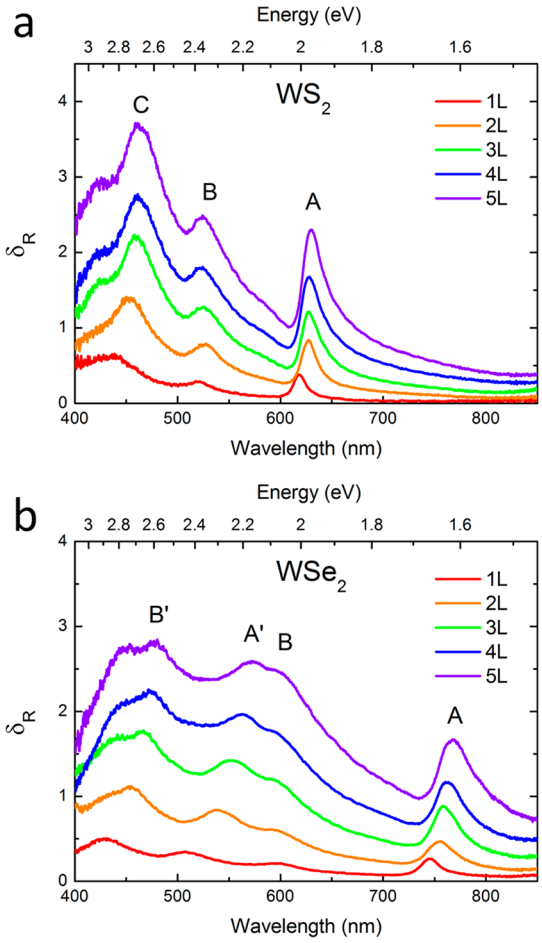

Figure 1. Differential reflectance spectra of mechanically exfoliated (a) 2H-WS_2 and (b) 2H-WSe_2 flakes consisting of 1−5 layers. The peaks are labeled according to the convention proposed by Wilson and Yoffe.[22]

substrate with refractive index of n_{subs} is related to the absorbance (A) of the material by[32]

$$\delta_R(\lambda) = \frac{4}{{n_{subs}}^2 - 1} A(\lambda) \quad (1)$$

We assume n_{subs} to be wavelength independent for the spectral range investigated in this study. Figure 1 panels a and b show the differential reflectance spectra of 1−5 layer WS_2 and WSe_2, respectively. Absorption features for bulk crystals have been previously studied by Beal *et al.*[33] and Bromley *et al.*[34] General features of the peaks are in good agreement with the previously reported results. All peaks exhibit a gradual but distinct blueshift with decreasing flake thickness similar to early findings.[35] Excitonic absorption peaks A and B which arise from direct gap transitions at the K point are found, respectively, around 625 and 550 nm for WS_2 and around 760 and 600 nm for WSe_2 in agreement with the previous studies on bulk layers.[33,34] The energy difference between the A and B peaks, which is an indication of the strength of spin−orbit interaction, is approximately 400 meV for both WS_2 and WSe_2 in reasonable agreement with the calculations.[36]

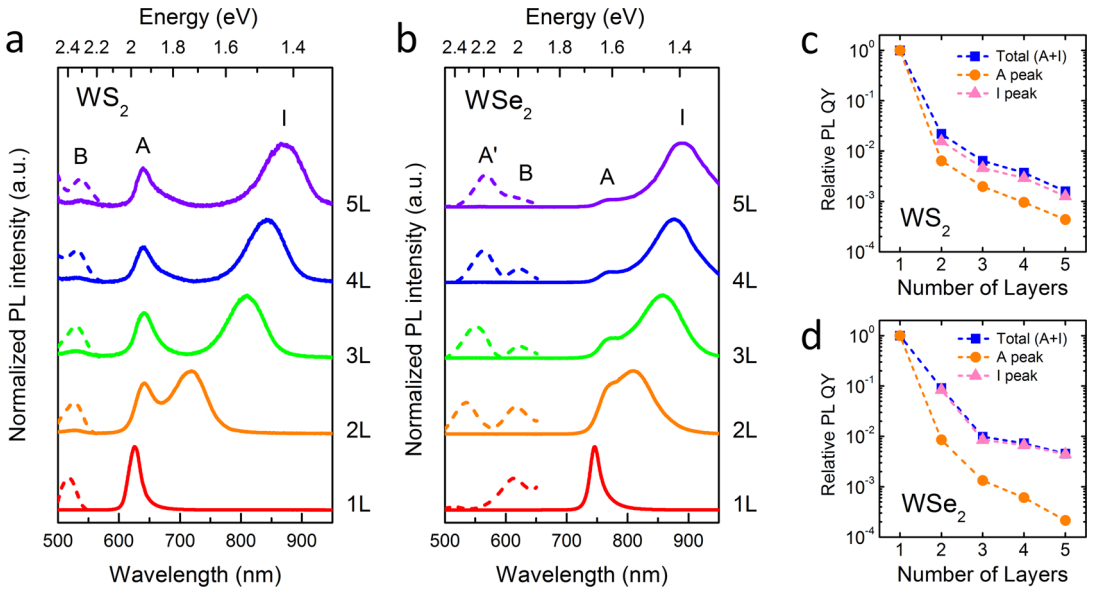

Figure 2. (a,b) Normalized PL spectra of mechanically exfoliated (a) 2H-WS_2 and (b) 2H-WSe_2 flakes consisting of 1−5 layers. Peak I is an indirect gap emission. Weak hot electron peaks A′ and B are magnified and shown as dashed lines for clarity. These hot electron peaks are typically 100 to 1000 times weaker than the band edge emission peaks. The total emission intensity becomes significantly weaker with increasing number of layers. (c,d) Relative decay in the PL QY with the number of layers for (c) WS_2 and (d) WSe_2. The values are relative to the PL QY of a monolayer flake as discussed in the text. The plots are shown for A and I peaks and their sum (A+I).

It should be noted that this value is significantly larger than the ∼160 meV splitting observed for MoS_2.[4,5]

For WS_2, an additional peak, previously labeled as C, is observed around 450 nm. This peak arises from optical transitions between the density of states peaks in the valence and conduction bands.[37] The WSe_2 spectra show more additional features due to greater overlap of Se p orbitals with W d orbitals as well as those of adjacent layers.[33,34] The absorption peaks A′ and B′ are believed to be excitonic in nature and arise from the splitting of the ground and excited states of A and B transitions, respectively, due to inter- and intralayer perturbation to the d electron band by the Se p orbitals.[33,34] The energy separation between A′ and B′ peaks are found to be ∼400 meV consistent with this picture. It may be noted that the presence of A′ and B′ peaks in monolayer WSe_2 suggests that A-A′ and B-B′ splitting are mainly due to intralayer effects.

In contrast to absorption, PL spectra show remarkable dependence on flake thickness for both materials as shown in Figure 2a,b. The most notable change is the sudden increase in emission intensity when the flake is thinned to a monolayer (Figure 2c,d). Both monolayer WS_2 and WSe_2 flakes exhibit strong emission at the energy corresponding to A excitonic absorption, whereas the emission intensity is dramatically reduced for multilayer flakes. While an accurate measurement of the PL quantum yield (QY) is challenging, relative changes in QY between different samples can be evaluated based on the PL and absorption spectra. Since the integrated PL intensity I is proportional to the product of $\alpha(\lambda_{exc})$ and QY, where $\alpha(\lambda_{exc})$ is the absorption coefficient at the excitation wavelength λ_{exc}, we can evaluate the relative magnitude of QY by comparing $I/\alpha(\lambda_{exc})$. Figure 2 panels c and d show relative decrease in PL QY with respect to monolayer flakes. For WS_2, PL QY drops by more than 100 folds when the thickness is increased from monolayer to bilayer and gradually diminishes with a further increase in thickness. A similar jump in PL QY was observed for WSe_2 although the changes between monolayer and bilayer flakes is less pronounced.

For A excitonic emission from monolayer WS_2 and WSe_2, Stokes shift was typically around 20 and 3 meV and the corresponding full width at half-maximum (fwhm) for these peaks was 75 and 26 meV, respectively (see Supporting Information for details). It is known that for quantum well structures, Stokes shift and emission line width are an indication of interfacial quality.[38] A recent study showed that the size of the Stokes shift in monolayer MoS_2 increases with doping concentration.[39] The narrow emission line, whose fwhm is comparable to thermal energy at room temperature, along with the small Stokes shift indicates the high quality of our WSe_2 samples.

In addition to the A exciton peak, another peak at a longer wavelength was observed for multilayer samples of both materials. This is attributed to indirect band gap emission involving a conduction band minimum at a midpoint between K and Γ points and valence band maximum at the Γ point. Calculations show that for WSe_2 bilayers, the indirect gap emission involves a valence band maximum at the κ point which is nearly degenerate with the band maximum at the

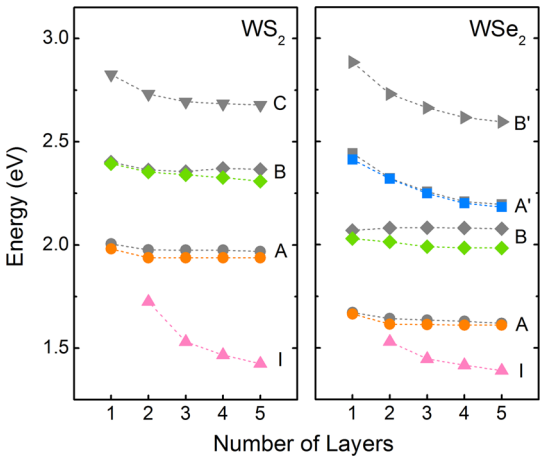

Figure 3. Absorption (gray) and PL (color-coded) peak energies of WS_2 and WSe_2 flakes as a function of the number of layers. The letters I, A, B, A′, B′, and C refer to the peaks labeled in Figures 1 and 2.

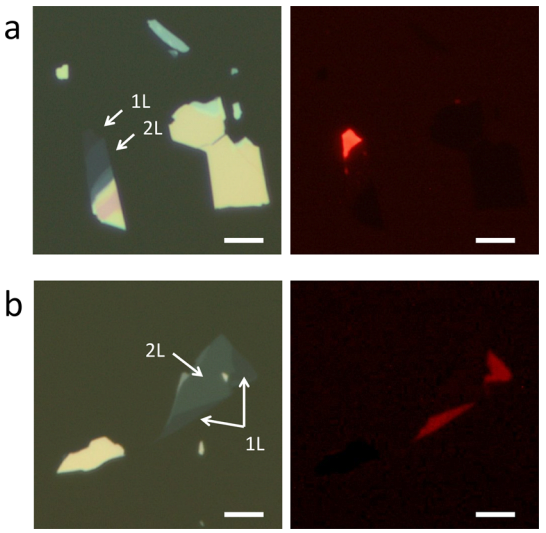

Figure 4. Bright field optical (left panels) and corresponding fluorescence (right panels) images of mechanically exfoliated (a) WS_2 and (b) WSe_2 flakes on a quartz substrate. The scale bar is 5 μm. The fluoresence images were obtained with excitation wavelength of 510−550 nm. Due to low efficiency of the CCD cameara in the NIR range, the fluorescence image contrast is artificially enhanced for WSe_2. The original image can be found in the Supporting Information.

Γ point.[26,40] It should be noted that the indirect gap emisision peak is virtually absent in the monolayer emission spectra, indicating that both WS_2 and WSe_2 become a direct gap semiconductor when they are thinned to a single monolayer. This observation along with the distinctly strong emission from monolayers is in good agreement with the calculated[25−27] results as well as the recent experimental findings.[28]

We observed that the decay in emission intensity with increasing thickness is more moderate for WSe_2 compared to WS_2. This is attributed to the small difference between the direct and indirect emission energies. For bulk WSe_2, the energy difference between the Γ and Κ points of the valence band was previously measured by photoemission spectroscopy to be <80 meV.[41,42] Theoritical calculations also yield similar results.[26,40] For bilayer WSe_2, the difference between the direct and indirect gaps is a measure of the energy separation between the conduction minimum at the Κ point and at a midpoint between Γ and K points. On the basis of our PL results we find this energy separation in bilayer WSe_2 to be about 70 meV. In comparison, the difference between the indirect and direct band gaps in bilayer WS_2 is much greater (∼300 meV). Because the population of hot electrons that transiently occupy the direct band edge at the K point is higher in bilayer WSe_2 than in bilayer WS_2 due to the smaller energy difference between its direct and indirect gaps, its A exciton hot electron emission is more pronounced. A similar scenario was recently reported for few-layer $MoSe_2$.[43]

For multilayer samples, the indirect gap emission intensity is comparable to or higher than that of hot electron emission from A excitons. We compared the indirect gap emission intensity of natural MoS_2 and our CVT-grown WX_2 multilayers and found that the emission intensity was consistently higher for the synthetic samples. Radiative recombination across an indirect gap is a slow process requiring phonons with an appropriate momentum. In the presence of defects acting as nonradiative traps, nonradiative decay will dominate and suppress the PL QY. Observation of comparatively strong indirect gap emission therefore provides further evidence that our CVT-grown samples are of high quality.

Figure 3 shows absorption and PL peak energies as a funtion of the number of layers. The A and B exciton peak positions are only weakly dependent on the flake thickness while the indirect band gap quickly decreases with increasing thickness. The robust direct gap at the Κ point (i.e. weakly thickness-dependent A and B transition energies) is attributed to the absence of dispersion in the out-of-plane direction (or large effective mass in the out-of-plane direction). On the other hand, out-of-plane dispersion around the Γ point (i.e. along the Γ-A line) and a midpoint between the Γ−K line is greater and results in thickness dependent indirect gap. Therefore, a large shift in absorption and emission peaks with flake thickness is an indication of out-of-plane dispersion or interlayer coupling of the electronic states involved in the transition. The energy of A, B, and C peaks in WS_2 and A and B peaks in WSe_2 are weakly dependent on the flake thickness indicating that the electrons localized within the plane of X-W-X sandwich are responsible for these optical transitions. For WSe_2, the shift in peaks A′ and B′ are more pronounced compared to that of peaks A and B suggesting that the electronic states associated with these optical transitions are more extended in the out-of-plane direction.

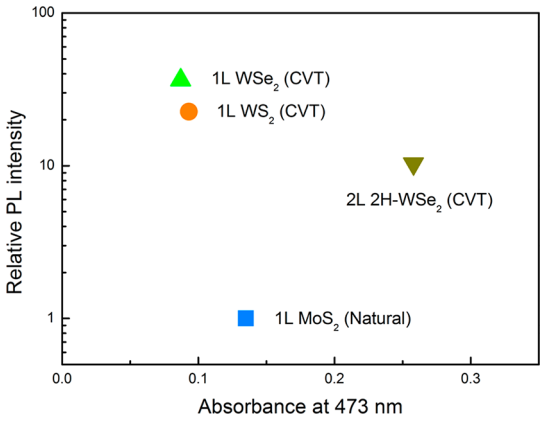

Figure 5. Relative integrated PL intensity of WS_2 and WSe_2 monolayers and WSe_2 bilayer with respect to that of a MoS_2 monolayer plotted against absorbance at the excitation wavelength of 473 nm. The PL emission spectra were integrated over 520−950 nm. Absorbance is obtained from differential reflectance of samples on quartz based on eq 1. The absorbance of MoS_2 is obtained from ref 5. Note that the comparison is made between exfoliated samples from synthetic (*i.e.*, CVT-grown) WS_2/WSe_2 and natural MoS_2 (SPI supplies) crystals.

Photoluminescence from monolayer flakes was sufficiently strong to be imaged under fluorescence microscope. Figure 4 shows bright field optical microscope images and corresponding fluorescence images of exfoliated WS_2 and WSe_2 flakes on quartz substrates. The fluorescence images clearly show red luminescence from the monolayer regions consistent with the PL spectrum. Emission intensity from the adjacent bilayer regions is not sufficiently strong to be imaged under the exposure condition used. The emission intensity is uniform across the monolayer region, verifying that the PL is not due to anomalies arising from flake edges. Similar fluorescence images were obtained for samples deposited on SiO_2/Si substrates (see Supporting Information). These results demonstrate that fluorescence imaging offers a powerful tool to quickly identifying monolayers.

Ideal direct band gap semiconductors are expected to exhibit high PL QY. However, the PL QY of the MoS_2 monolayer was previously found to be extremely low (4×10^{-3}).[5] The origin of the low QY is yet to be understood. Unintentional doping in the natural crystals with an estimated concentration of $\sim 10^{12}$ cm^{-2} [1,6,18] may play a role in suppressing exciton formation and/or its radiative recombination.[44,45] Figure 5 shows a relative comparison of the emission intensity from exfoliated MoS_2, WS_2 and WSe_2. The emission intensity of our monolayer WS_2 and WSe_2 is 20 to 40 times higher than that of monolayer MoS_2 exfoliated from a natural crystal. The emission from bilayer WSe_2 is also more efficient in comparison to monolayer MoS_2. The differences in PL QY may arise due to various intrinsic and extrinsic factors. We suspect that the observed differences in PL QY mainly arise from unintentional doping in our samples. Further studies are required to elucidate the origin of the variations in PL QY reported here.

CONCLUSIONS

In summary, we studied the evolution of electronic structure in atomically thin WS_2 and WSe_2 sheets using differential reflectance and PL spectroscopy. Our results demonstrate that indirect-to-direct gap crossover occurs in these materials when they are thinned to a single monolayer similar to the case of MoS_2. Due to direct gap excitonic recombination, strongly enhanced PL centered at 630 and 750 nm is observed from monolayer WS_2 and WSe_2, respectively. The emission from monolayers is 100 to 1000 times stronger than from the bulk materials. The high quality of our CVT-grown samples is suggested by the distinct indirect gap emission, small Stokes shift, and narrow emission line width. Enhanced interlayer coupling in WSe_2 is suggested by the pronounced thickness-dependent shift of A′ and B′ absorption and emission peaks.

Our findings demonstrate the unique variations in the optical properties of 2D semiconducting crystals belonging to the family of group 6 LTMDs. Structual similarities of these materials allows fabrication of coherent artificial crystals consisting of electronically dissimilar layers.[46−48] Monolayer WS_2 and WSe_2 with direct band gap in the visible and NIR frequency ranges, respectively, are novel building blocks for realizing unique heterostructures with tailored optoelectronic, electrocatalytic, and photocatalytic functionalities.[49]

METHOD

Synthetic crystals of 2H-WS_2 and 2H-WSe_2 were grown by the chemical vapor transport (CVT) method using iodine as the transport agent. Commercial natural 2H-MoS_2 (SPI Supplies) was studied for comparison. The crystals were mechanically exfoliated and deposited on quartz and SiO_2/Si substrates for subsequent characterizations. Regions of the sample containing mono- and few-layer sheets were first identified under optical microscope and the number of layers was verified by atomic force microscope (AFM) and optical contrast. Differential reflectance measurements were performed using a Jobin-Yvon HR800 micro-Raman system equipped with a liquid nitrogen cooled charge-coupled detector. A tungsten-halogen lamp was used as a light source. Differential reflectance is defined as $1 - R_S/R_Q$, where R_S and R_Q are the reflected light intensities from the quartz substrate with and without WS_2/WSe_2 flake samples, respectively. The light illuminating the sample was focused down to a 1 μm spot using a small confocal hole. The spectra acquisition time was 15 s. The intensity of the light incident on the sample was kept low (<1 mW) in order to avoid sample damage. Photoluminescence spectra were obtained in a back scattering geometry with a 473 nm excitation laser at intensities less than 150 μW. The fluorencence images were obtained with an Olympus fluorencence microscope equipped with a Mercury lamp as the excitation light source.

Conflict of Interest: The authors declare no competing financial interest.

Acknowledgment. G. Eda acknowledges Singapore National Research Foundation for funding the research under NRF Research Fellowship (NRF-NRFF2011-02). P. H. Tan acknowledges the support from NSFC under Grants 10934007 and 11225421.

Supporting Information Available: Atomic force microscope (AFM) results, fluorescence microscope images, and additional photoluminescence spectra showing Stokes shift. This material is available free of charge *via* the Internet at http://pubs.acs.org.

REFERENCES AND NOTES

1. Radisavljevic, B.; Radenovic, A.; Brivio, J.; Giacometti, V.; Kis, A. Single-Layer MoS_2 Transistors. *Nat. Nanotechnol.* **2011**, *6*, 147–150.
2. Lembke, D.; Kis, A. Breakdown of High-Performance Monolayer MoS_2 Transistors. *ACS Nano* **2012**, *6*, 10070–10075.
3. Liu, H.; Neal, A. T.; Ye, P. D. Channel Length Scaling of MoS_2 Mosfets. *ACS Nano* **2012**, *6*, 8563–8569.
4. Splendiani, A.; Sun, L.; Zhang, Y.; Li, T.; Kim, J.; Chim, C.-Y.; Galli, G.; Wang, F. Emerging Photoluminescence in Monolayer MoS_2. *Nano Lett.* **2010**, *10*, 1271–1275.
5. Mak, K. F.; Lee, C.; Hone, J.; Shan, J.; Heinz, T. F. Atomically Thin MoS_2: A New Direct-Gap Semiconductor. *Phys. Rev. Lett.* **2010**, *105*, 136805.
6. Mak, K. F.; He, K.; Shan, J.; Heinz, T. F. Control of Valley Polarization in Monolayer MoS_2 by Optical Helicity. *Nat. Nanotechnol.* **2012**, *7*, 494–498.
7. Zeng, H.; Dai, J.; Yao, W.; Xiao, D.; Cui, X. Valley Polarization in MoS_2 Monolayers by Optical Pumping. *Nat. Nanotechnol.* **2012**, *7*, 490–493.
8. Cao, T.; Wang, G.; Han, W.; Ye, H.; Zhu, C.; Shi, J.; Niu, Q.; Tan, P.; Wang, E.; Liu, B.; *et al.* Valley-Selective Circular Dichroism of Monolayer Molybdenum Disulphide. *Nat. Commun.* **2012**, *3*, 887.
9. Bertolazzi, S.; Brivio, J.; Kis, A. Stretching and Breaking of Ultrathin MoS_2. *ACS Nano* **2011**, *5*, 9703–9709.
10. Yin, Z.; Li, H.; Li, H.; Jiang, L.; Shi, Y.; Sun, Y.; Lu, G.; Zhang, Q.; Chen, X.; Zhang, H. Single-Layer MoS_2 Phototransistors. *ACS Nano* **2012**, *6*, 74–80.
11. Radisavljevic, B.; Whitwick, M. B.; Kis, A. Integrated Circuits and Logic Operations Based on Single-Layer MoS_2. *ACS Nano* **2011**, *5*, 9934–9938.
12. Kim, S.; Konar, A.; Hwang, W.-S.; Lee, J. H.; Lee, J.; Yang, J.; Jung, C.; Kim, H.; Yoo, J.-B.; Choi, J.-Y.; *et al.* High-Mobility and Low-Power Thin-Film Transistors Based on Multilayer MoS_2 Crystals. *Nat. Commun.* **2012**, *3*, 1011.
13. Wang, H.; Yu, L.; Lee, Y.-H.; Shi, Y.; Hsu, A.; Chin, M. L.; Li, L.-J.; Dubey, M.; Kong, J.; Palacios, T. Integrated Circuits Based on Bilayer MoS_2 Transistors. *Nano Lett.* **2012**, *12*, 4674–4680.
14. Li, H.; Yin, Z.; He, Q.; Li, H.; Huang, X.; Lu, G.; Fam, D. W. H.; Tok, A. I. Y.; Zhang, Q.; Zhang, H. Fabrication of Single- and Multilayer MoS_2 Film-Based Field-Effect Transistors for Sensing Not at Room Temperature. *Small* **2012**, *8*, 63–67.
15. Pu, J.; Yomogida, Y.; Liu, K.-K.; Li, L.-J.; Iwasa, Y.; Takenobu, T. Highly Flexible MoS_2 Thin-Film Transistors with Ion Gel Dielectrics. *Nano Lett.* **2012**, *12*, 4013–4017.
16. He, Q.; Zeng, Z.; Yin, Z.; Li, H.; Wu, S.; Huang, X.; Zhang, H. Fabrication of Flexible MoS_2 Thin-Film Transistor Arrays for Practical Gas-Sensing Applications. *Small* **2012**, *8*, 2994–2999.
17. Lee, H. S.; Min, S.-W.; Chang, Y.-G.; Park, M. K.; Nam, T.; Kim, H.; Kim, J. H.; Ryu, S.; Im, S. MoS_2 Nanosheet Phototransistors with Thickness-Modulated Optical Energy Gap. *Nano Lett.* **2012**, *12*, 3695–3700.
18. Zhang, Y.; Ye, J.; Matsuhashi, Y.; Iwasa, Y. Ambipolar MoS_2 Thin Flake Transistors. *Nano Lett.* **2012**, *12*, 1136–1140.
19. Novoselov, K. S.; Jiang, D.; Schedin, F.; Booth, T. J.; Khotkevich, V. V.; Morozov, S. V.; Geim, A. K. Two-Dimensional Atomic Crystals. *Proc. Nat. Acad. Sci. U.S.A.* **2005**, *102*, 10451–10453.
20. Goldberg, A. M.; Beal, A. R.; Lévy, F. A.; Davis, E. A. The Low-Energy Absorption Edge in 2H-MoS_2 and 2H-$MoSe_2$. *Philos. Mag.* **1975**, *32*, 367–378.
21. Neville, R. A.; Evans, B. L. Band Edge Excitons in 2h-MoS_2. *Phys. Stat. Sol. B* **1976**, *73*, 597–606.
22. Wilson, J. A.; Yoffe, A. D. The Transition Metal Dichalcogenides: Discussion and Interpretation of the Observed Optical, Electrical and Structural Properties. *Adv. Phys.* **1969**, *18*, 193–335.
23. Braga, D.; Gutiérrez Lezama, I.; Berger, H.; Morpurgo, A. F. Quantitative Determination of the Band Gap of WS_2 with Ambipolar Ionic Liquid-Gated Transistors. *Nano Lett.* **2012**, *12*, 5218–5223.
24. Fang, H.; Chuang, S.; Chang, T. C.; Takei, K.; Takahashi, T.; Javey, A. High-Performance Single Layered WSe_2 p-FETs with Chemically Doped Contacts. *Nano Lett.* **2012**, *12*, 3788–3792.
25. Kuc, A.; Zibouche, N.; Heine, T. Influence of Quantum Confinement on the Electronic Structure of the Transition Metal Sulfide TS_2. *Phys. Rev. B* **2011**, *83*, 245213.
26. Yun, W. S.; Han, S. W.; Hong, S. C.; Kim, I. G.; Lee, J. D. Thickness and Strain Effects on Electronic Structures of Transition Metal Dichalcogenides: 2H-MX_2 Semiconductors (M = Mo, W; X = S, Se, Te). *Phys. Rev. B* **2012**, *85*, 033305.
27. Jiang, H. Electronic Band Structures of Molybdenum and Tungsten Dichalcogenides by the GW Approach. *J. Phys. Chem. C* **2012**, *116*, 7664–7671.
28. Zeng, H.; Liu, G.-B.; Dai, J.; Yan, Y.; Zhu, B.; He, R.; Xie, L.; Xu, S.; Chen, X.; Yao, W., *et al.* Optical Signature of Symmetry Variations and Spin-Valley Coupling in Atomically Thin Tungsten Dichalcogenides. *arXiv:1208.5864*, submitted 29 Aug 2012.
29. Gutierrez, H. R.; Perea-Lopez, N.; Elias, A. L.; Berkdemir, A.; Wang, B.; Lv, R.; Lopez-Urias, F.; Crespi, V. H.; Terrones, H.; Terrones, M., Extraordinary Room-Temperature Photoluminescence in WS_2 Triangular Monolayers. *Nano Lett.* **2012**, DOI: 10.1021/nl3026357.
30. Li, H.; Lu, G.; Yin, Z.; He, Q.; Li, H.; Zhang, Q.; Zhang, H. Optical Identification of Single- and Few-Layer MoS_2 Sheets. *Small* **2012**, *8*, 682–686.
31. Zhao, W. Manuscript in preparation.
32. Hecht, E. *Optics*; Addison-Wesley: Reading, MA, 1998.
33. Beal, A. R.; Knights, J. C.; Liang, W. Y. Transmission Spectra of Some Transition Metal Dichalcogenides. II. Group VIA: Trigonal Prismatic Coordination. *J. Phys. C: Sol. Stat. Phys.* **1972**, *5*, 3540.
34. Bromley, R. A.; Murray, R. B.; Yoffe, A. D. The Band Structures of Some Transition Metal Dichalcogenides. III. Group VIA: Trigonal Prism Materials. *J. Phys. C: Sol. Stat. Phys.* **1972**, *5*, 759.
35. Consadori, F.; Frindt, R. F. Crystal Size Effects on the Exciton Absorption Spectrum of WSe_2. *Phys. Rev. B* **1970**, *2*, 4893–4896.
36. Ramasubramaniam, A. Large Excitonic Effects in Monolayers of Molybdenum and Tungsten Dichalcogenides. *Phys. Rev. B* **2012**, *86*, 115409.
37. Mattheis, L. F. Band Structures of Transition-Metal-Dichalcogenide Layer Compounds. *Phys. Rev. B* **1973**, *8*, 3719–3740.
38. Yang, F.; Wilkinson, M.; Austin, E. J.; O'Donnell, K. P. Origin of the Stokes Shift: A Geometrical Model of Exciton Spectra in 2D Semiconductors. *Phys. Rev. Lett.* **1993**, *70*, 323–326.
39. Mak, K. F.; He, K.; Lee, C.; Lee, G. H.; Hone, J.; Heinz, T. F.; Shan, J., Observation of Tightly Bound Trions in Monolayer Mos_2. *Nature Mater.* **2012**, DOI: 10.1038/nmat3505.
40. Voß, D.; Krüger, P.; Mazur, A.; Pollmann, J. Atomic and Electronic Structure of WSe_2 from *ab Initio* Theory: Bulk Crystal and Thin Film Systems. *Phys. Rev. B* **1999**, *60*, 14311–14317.
41. Finteis, T.; Hengsberger, M.; Straub, T.; Fauth, K.; Claessen, R.; Auer, P.; Steiner, P.; Hüfner, S.; Blaha, P.; Vögt, M.; *et al.* Occupied and Unoccupied Electronic Band Structure of WSe_2. *Phys. Rev. B* **1997**, *55*, 10400–10411.
42. Traving, M.; Boehme, M.; Kipp, L.; Skibowski, M.; Starrost, F.; Krasovskii, E. E.; Perlov, A.; Schattke, W. Electronic Structure of WSe_2: A Combined Photoemission and Inverse Photoemission Study. *Phys. Rev. B* **1997**, *55*, 10392–10399.

43. Tongay, S.; Zhou, J.; Ataca, C.; Lo, K.; Matthews, T. S.; Li, J.; Grossman, J. C.; Wu, J., Thermally Driven Crossover from Indirect toward Direct Bandgap in 2D Semiconductors: $MoSe_2$ *versus* MoS_2. *Nano Lett.* **2012**, *12*, 5576−5580.
44. Wu, S.; Ross, J. S.; Aivazian, G.; Jones, A.; Fei, Z.; Liu, G.-B.; Zhu, W.; Xiao, D.; Yao, W.; Cobden, D., *et al*. Electrical Tuning of Valley Magnetic Moment *via* Symmetry Control. *arXiv:1208.6069*, submitted 30 August, 2012.
45. Newaz, A. K. M.; Prasai, D.; Ziegler, J. I.; Caudel, D.; Robinson, S.; Jr, R. F. H.; Bolotin, K. I., Electrical Control of Optical Properties of Monolayer MoS_2. *Solid State Commun*. **2013**, *155*, 49−52.
46. Novoselov, K. S.; Neto, A. H. C. Two-Dimensional Crystals-Based Heterostructures: Materials with Tailored Properties. *Phys. Scr.* **2012**, *2012*, 014006.
47. Gao, G.; Gao, W.; Cannuccia, E.; Taha-Tijerina, J.; Balicas, L.; Mathkar, A.; Narayanan, T. N.; Liu, Z.; Gupta, B. K.; Peng, J.; *et al*. Artificially Stacked Atomic Layers: Toward New van Der Waals Solids. *Nano Lett.* **2012**, *12*, 3518–3525.
48. Bernardi, M.; Palummo, M.; Grossman, J. C., Semiconducting Monolayer Materials as a Tunable Platform for Excitonic Solar Cells. *ACS Nano* **2012**, *6*, 10082−10089.
49. Wang, Q. H.; Kalantar-Zadeh, K.; Kis, A.; Coleman, J. N.; Strano, M. S. Electronics and Optoelectronics of Two-Dimensional Transition Metal Dichalcogenides. *Nat. Nanotechnol.* **2012**, *7*, 699–712.